Journal Name

ARTICLE TYPE

Cite this: DOI: 10.1039/xxxxxxxxxx

Investigating the electronic structure of a supported metal nanoparticle: Pd in SiCN

Tobias Schmidt,[a] Rodrigo Q. Albuquerque,[bc] Rhett Kempe,[d] and Stephan Kümmel*[a]

We investigate the electronic structure of a Palladium nanoparticle that is partially embedded in a matrix of silicon carbonitride. From classical molecular dynamics simulations we first obtain a representative atomic structure. This geometry then serves as input to density-functional theory calculations that allow us to access the electronic structure of the combined system of particle and matrix. In order to make the computations feasible, we devise a subsystem strategy for calculating the relevant electronic properties. We analyze the Kohn-Sham density of states and pay particular attention to d-states which are prone to be affected by electronic self-interaction. We find that the density of states close to the Fermi level is dominated by states that originate from the Palladium nanoparticle. The matrix has little direct effect on the electronic structure of the metal. Our results contribute to explaining why silicon carbonitride does not have detrimental effects on the catalytic properties of palladium particles and can serve positively as a stabilizing mechanical support.

1 Motivation

First-principles electronic-structure theory[1–13] allows to gain unbiased insights into the microscopic, quantum-mechanical effects that are at the heart of modern nanotechnology[14–24]. However, often full *ab-initio* studies on systems of experimental relevance remain challenging since the computational effort grows immensely with system size[25]. For instance, in many experiments metal nanoparticles that have a diameter of several nm and contain several hundreds or thousands of atoms are used. For such systems, tens of thousands of electrons have to be taken into account for first-principles studies. Even with modern computers using massive parallelization, geometry optimizations and detailed investigations of the electronic structure of systems of that size are out of reach. Therefore, strategies have to be devised how insights can be gained into large systems despite of these computational limitations. In this work, we take a first step in this direction and investigate a palladium nanoparticle which is partially embedded in a matrix of silicon carbonitride (SiCN).

This system is of practical relevance because noble-metal nanoparticles, in particular nanoparticles containing Pd, are effective catalysts for a wide range of chemical reactions[26–30]. In comparison to bulk metals, nanoparticles exhibit a high surface-to-volume ratio and active atoms at the surface, resulting in a high chemical activity[31,32]. However, the use of plain nanoparticles as catalysts suffers from practical limitations such as aggregation and deactivation during the reaction, resulting in an undesired loss of their catalytic activity and an insufficient reusability[33].

These limitations can be addressed by embedding the metal nanoparticles in a solid supporting material[34]. Supported metal nanoparticles (SMNPs) offer great advantages such as, for instance, a high thermal and mechanical stability as well as long-term durability[32]. Since SMNPs facilitate an effortless removal from the reaction medium and prevent aggregation, they equip the catalytic material with a higher reusability[32]. In particular the concept of using a SiCN matrix has proven to be promising for the design of SMNPs[35,36]. It was reported that SiCN-based SMNPs (denoted "M@SiCN", with "M" denoting the metal of which the nanoparticle is composed) yield materials that are robust under thermal and mechanical influences, while maintaining a high chemical stability[37–41]. Thus, SiCN provides reliable support for heterogeneous catalysts such as, for instance, Pd@SiCN[41], resulting in a stable and highly reusable catalytic material for a manifold of chemical reactions[37,39,42,43].

In this paper, we take a look at Pd@SiCN from a theoretical point of view. In particular, we investigate the influence of the SiCN support on the electronic structure of a Pd nanoparticle with a focus on properties that are typically related to catalytic activity. For this, we explicitly consider a Pd nanoparticle with a diamater of ≈ 3 nm, containing a total of 586 Pd atoms. This nanoparticle is partially embedded in a matrix of 2240 Si, 1904 C, and 2140 N atoms, a ratio that resembles typical experimental situa-

[a] *Theoretical Physics IV, University of Bayreuth, 95440 Bayreuth, Germany. E-mail: stephan.kuemmel@uni-bayreuth.de*
[b] *São Carlos Institute of Chemistry, University of São Paulo, 13560-970 São Carlos (SP), Brazil.*
[c] *School of Pharmacy & Biomolecular Sciences, Liverpool John Moores University, L3 3AF Liverpool, UK.*
[d] *Inorganic Chemistry II, University of Bayreuth, 95440 Bayreuth, Germany.*

tions. Due to the large number of atoms involved, ground-state density-functional theory (DFT)[44–46] is the method of choice for electronic-structure calculations on Pd@SiCN. Unfortunately, it is not feasible to include all 6870 atoms, many of which belong to a transition metal with a substantial number of valence electrons, in a DFT calculation for the whole system.

Therefore, we present a computational strategy to effectively access the relevant electronic-structure properties of SMNPs by employing a combination of methods: First, the geometry of the embedded Pd nanoparticle is obtained by classical molecular-dynamics (MD) simulations. Using the MD structure, we divide the SMNP into subsystems of varying sizes around a reference point at the Pd-SiCN interface. We then calculate the electronic structure of representative subsystems with DFT. In particular, we focus on the calculated density of states (DOS) close to the Fermi edge as a general indicator for the chemical activity of the nanoparticle[19,21,30]. We separate the influence of the support on the electronic structure of the nanoparticle by explicitly calculating the DOS for the combined Pd@SiCN and contrast it with pure Pd and pure SiCN of the same geometry.

In order to be sure about the reliability of our electronic structure results we calculate the DOS with different density functionals. Primarily we use the generalized gradient approximation of Perdew-Burke-Ernzerhof (PBE)[47,48]. However, we address the question of electronic self-interaction[49], which may affect the energetic position of states emerging from localized d-states[50], by also evaluating the DOS with the PBE0[51] and BHLYP[52] hybrid functionals. These partially counteract self-interaction[50,53,54]. We thus ensure that the influence of the support on the electronic structure of the nanoparticle is not merely a feature observed for a particular density functional, but is truly of systematic character.

This paper is organized as follows: in Sec. 2 we provide details on the MD simulations of Pd@SiCN and present the obtained geometry. The subsystem approach is introduced and discussed in Sec. 3. In Sec. 4 we analyze the DOS for representative subsystems and characterize the influence of the supporting material on the electronic structure of the Pd nanoparticle. We discuss the implications of our findings for the theoretical investigations of SMNPs in general and for the practical use of Pd@SiCN as a catalytic material in Sec. 5.

2 Molecular-Dynamics Simulations

One strategy for obtaining the structure of a Pd particle on a SiCN support would be to use global optimization methods or schemes like the Wulff-Kaischew construction[55,56] to find low energy geometries. However, for a system as large as the one that we consider here, global optimization techniques would be computationally overwhelming and would most likely lead to a very large number of local minima. Furthermore, due to the amorphous character of our system, strategies based on crystal structures and symmetries are not applicable. However, this is not a problem for the present study, because our focus is not on finding the one lowest energy structure, but on obtaining a structure that is reasonably close to a typical experimental situation. As the experimental conditions[41] can be expected to produce structures that share global characteristics but differ in their detailed structure, the focus is on reproducing the relevant global characteristics.

Therefore, as a starting point to our investigations, the structure of one supported Pd nanoparticle embedded in SiCN was calculated using classical MD simulations. Initially, the Pd nanoparticle was taken as a cutout from the fcc bulk crystal lattice containing 586 Pd atoms, which is a magic number for a truncated octahedron of about 3 nm in diameter. This cutout was then half-embedded in a matrix of randomly distributed atoms (2240 Si, 1904 C, and 2140 N) in a box of $5.4 \times 5.6 \times 2.6$ nm, leading to a total of 6870 atoms in the simulation box. We have chosen to adsorb the Pd NP onto the SiCN substrate via the 111 facet, which is in agreement with the preferred epitaxy reported for other Pd-supported systems[56].

The interactions between the Pd atoms within the nanoparticle were computed using the well-known embedded-atom model[57], while the interactions within the SiCN matrix were simulated using the Tersoff potential[58–60]. The interactions between the atoms of the support and the nanoparticle were computed based exclusively on a Lennard-Jones potential, whose parameters were previously optimized using DFT (PBE0/LANL2DZ/6-31G*) calculations. Periodic boundary conditions were applied to the x and y directions and the NPT ensemble was adopted. All MD simulations were carried out using the `LAMMPS` program package[61] with timesteps of 1 fs. The full system Pd@SiCN was initially heated up to 300 K under 1 atm and then slowly cooled down to 10 K at a cooling rate of 0.00036 K/step. The final structure was taken as the atomic configuration to be used as an input to the DFT calculations. The obtained structure is shown in Fig. 1.

As can be seen in panel (a) and (b) of Fig. 1, the half-embedded Pd particle is somewhat deformed due to the interaction with the SiCN support. At the base its overall diameter is ca. 3 nm. The nanoparticle extends to ca. 0.5 nm into the SiCN support, and its height is ca. 2 nm above the SiCN surface. Importantly, the Pd particle clearly retains an organized, faceted structure in the center. Thus, the result of the MD simulation captures decisive features observed in experimental situations[41].

In order to investigate the influence of the support on the electronic properties of the Pd nanoparticle, however, it is necessary to access the system's electronic structure. This cannot be achieved with classical MD simulations. However, the combined total system Pd@SiCN is considerably too large for a straightforward DFT calculation. In the following we therefore devise a systematic scheme for selecting computationally manageable yet representative subsystems from the total Pd@SiCN system.

3 The Subsystem Approach

The challenge that we need to address is the following: For reasons of computational feasibility we can run DFT calculations not for the total Pd@SiCN system, but only for a part of it. This part, however, needs to be chosen such that it is representative of the full system. To ensure that this is the case, we need some test of "convergence" that allows us to estimate whether the subsystem that we chose is sufficiently large to be representative.

We solved this problem by creating a set of subsystems according to the following strategy: First, a reference point was chosen

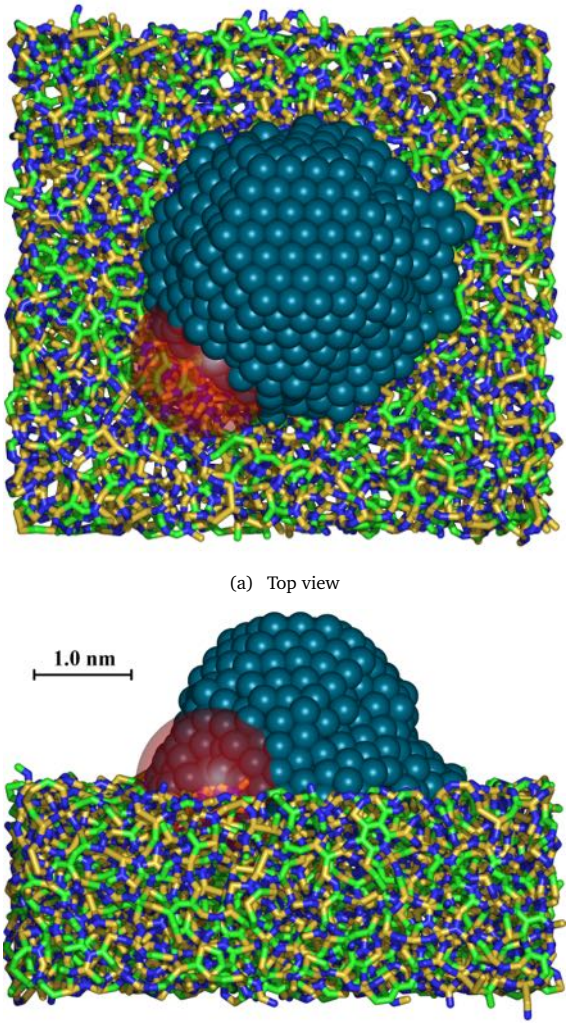

(a) Top view

(b) Front view

Fig. 1 Structure of the SMNP Pd@SiCN as obtained by the MD simulation. Palladium atoms are represented in metallic blue, silicon in yellow, carbon in green, and nitrogen in blue. The red, semitransparent sphere marks the subsystem with a radius of $R = 8.0$ taken around the reference point at the Pd-SiCN interface.

at the interface of the nanoparticle and the matrix as detailed below. This reference point serves as the center of a sphere with radius R. Each subsystem is then defined by its sphere radius and contains all atoms that are located within this particular sphere. (*cf.* Fig. 1, which shows the subsystem with $R = 8.0$ around the reference point as an example). In principle, for very large R, eventually all atoms would be included in the sphere and the calculation for the atoms within the sphere is then identical to a calculation for the entire system, i.e., the subsystem procedure converges to the right limit with increasing R.

In the next step, DFT calculations were performed for subsystems of increasing size. In order to ensure that the subsystem approach leads to results that reliably represent the behavior of the overall system, the essential electronic-structure properties have to be investigated for convergence with respect to the sphere radius. In particular, we used the quantity

$$\Sigma_\Delta(R) = \frac{1}{N(R)} \int_{\varepsilon_{\text{Fermi}}-\Delta}^{\varepsilon_{\text{Fermi}}} g_R(\varepsilon)\, \mathrm{d}\varepsilon \qquad (1)$$

as an indicator for the behavior of the DOS in a certain energetic range Δ under the Fermi level $\varepsilon_{\text{Fermi}}$ (i.e. the energetic position of the highest occupied Kohn-Sham eigenvalue). The function $g_R(\varepsilon)$ denotes the DOS as obtained by a DFT calculation for a particular subsystem with radius R. It was obtained by convolving the calculated spectrum of occupied Kohn-Sham eigenvalues with Gaussians of a width of 0.08 eV. $N(R)$ denotes the total number of atoms involved in the respective subsystem. The quantity Σ_Δ as defined in Eq. 1 was chosen because the DOS right below the Fermi level is typically indicative for the chemical activity of the corresponding system and, consequently, can be regarded as the relevant electronic-structure property[30]. We divide by the number of atoms for normalization reasons. Thus, values of Σ_Δ for different values of R become comparable.

The choice of the reference point is an important part of the subsystem approach. It must be chosen such that all subsystems are, as good as possible, representative for the total system. The location of the reference point shown in Fig. 1 was chosen according to two criteria: First, the reference point was placed on the Pd-SiCN interface. Thus all subsystems contain chemically active surface atoms, i.e., those atoms that are of relevance for the question of how strongly the Pd nanoparticle interacts with the SiCN matrix. Second, we required that the ratio of Pd to SiCN atoms was approximately the same in all subsystems (i.e., for different radii). In this way we ensure that the different subsystems are comparable in terms of chemical composition. We further elaborate on this criterion in Appendix A, where we demonstrate that the number of atoms and electrons of type Pd, SiCN, and the combined Pd@SiCN indeed scale similarly with the sphere radius.

We further note that we used this strategy to set up different types of subsystems. Of primary interest are, of course, the systems that consist of Pd and SiCN, as just described. However, for analysis purposes we also created subsystems of pure Pd by taking the Pd@SiCN subsystems and removing all Si, C, and N atoms, or vice versa, i.e., creating pure SiCN systems by removing all Pd atoms. In doing so we deliberately did not perform any subsequent geometry optimization because we wanted to ensure that all changes observed in the DOS are of direct electronic origin, and not an indirect consequence of geometry changes.

We used the program package `TURBOMOLE`[62] to perform self-consistent DFT calculations. The PBE functional was utilized with a def2-TZVPP basis set, while the hybrid functionals were evaluated using a def2-SVP basis set in a generalized Kohn-Sham scheme[63]. We checked the accuracy of both the basis sets and the resolution-of-identity approximation (see Ref.[64] and references therein) and found that they have negligible influence on the quantity $\Sigma_\Delta(R)$.

Even with the introduction of subsystems the electronic-structure calculations remained challenging. However, using the semilocal functional PBE, convergence could be reached for subsystems sizes up to $R = 8.0$, which involved the explicit consideration of a total of 1940 electrons for Pd@SiCN. Calculations of

the combined system Pd@SiCN using the hybrid PBE0 could be converged up to a size of $R = 6.0$, in which case 890 electrons were considered. The obtained results for the integrated DOS as defined by Eq. 1 are given for $\Delta = 1$ eV in panel (a) and for $\Delta = 2$ eV in panel (b) of Fig. 2.

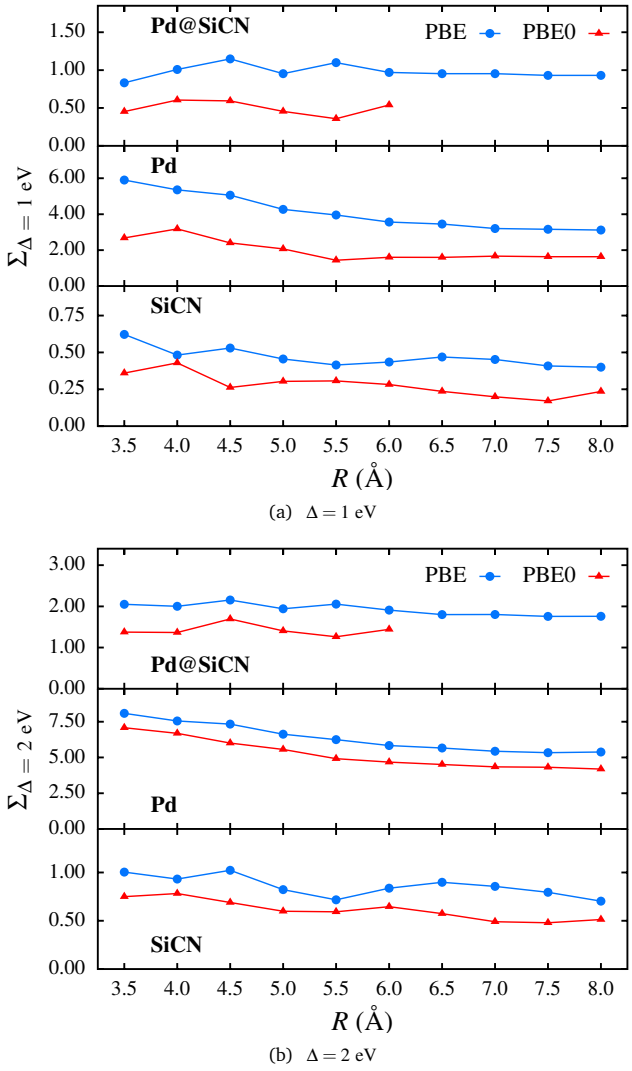

Fig. 2 Integrated DOS $\Sigma_\Delta(R)$ as a function of the subsystem radius R as obtained with PBE and PBE0 for the atoms of type Pd, SiCN, and the combined Pd@SiCN.

The results for the integrated DOS clearly indicate that Σ_Δ reaches convergence for the PBE and, in case of only Pd and SiCN, for the PBE0 functional for subsystem sizes above $R = 6.5 - 7.0$. This becomes clear because the lines level off and become horizontal beyond these values of R. The observations is further confirmed by extending the integration region from $\Delta = 1$ eV to $\Delta = 2$ eV. Consequently, subsystems of sufficient size give a reasonably reliable impression of the DOS of the Pd@SiCN system and it appears justified to access the electronic structure of the embedded nanoparticle by investigating representative subsystems.

4 Analyzing the Density of States

For the subsystem with $R = 8.0$, which, as argued above, can be considered as converged with respect to Σ_Δ, the complete DOS as obtained with PBE is shown in Fig. 3(a). The figure contains the occupied DOS for the combined system Pd@SiCN, for only Pd with all SiCN atoms removed, and for only SiCN with all Pd atoms removed.

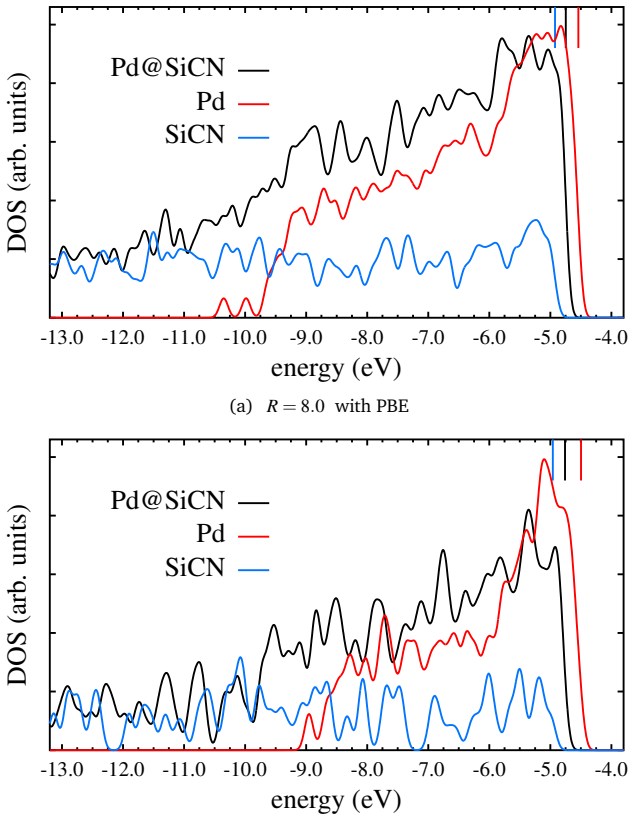

Fig. 3 Occupied part of the DFT DOS obtained with PBE for the subsystems with $R = 8.0$ (a) and $R = 5.5$ (b) for Pd only (red line), SiCN only (blue), and the combined Pd@SiCN (black). The position of the highest occupied KS states, i.e., the Fermi levels, are denoted by the colored ticks at the top of each graph.

It can clearly be seen that the DOS in the chemically most relevant region, i.e., the energetic domain close to the Fermi level, is dominated by the DOS originating from the Pd atoms. In this region, both the graphs of the combined Pd@SiCN and only Pd exhibit a similar structure and height, whereas the DOS of only SiCN has little resemblance to the corresponding curve of Pd@SiCN. Thus, it appears that the SiCN support does not interfere with the electronic structure of the Pd atoms. Therefore, one can argue that the electronic properties of the Pd nanoparticle are only weakly affected by the embedment.

A similar observation can be made for the results of the PBE calculation of a smaller subsystem with $R = 5.5$, which is shown in Fig. 3(b). Also in this case, the DOS close to the Fermi level is clearly dominated by the contribution from the Pd atoms, although the features in this case appear less distinct in detail.

We further support the conclusion that Pd retains its important electronic-structure properties by recalculating the smaller subsystem with $R = 5.5$ using different approximations for the exchange-correlation energy in the DFT calculations. In this way, we exclude the possibility that the observations based on Fig. 3 are merely features of the PBE functional, but rather are systematic results that are reproduced by other functional approximations. As mentioned above, hybrid functionals are of particular interest in this case. Fig. 4(a) shows the DOS for PBE0 and Fig. 4(b) the DOS for BHLYP.

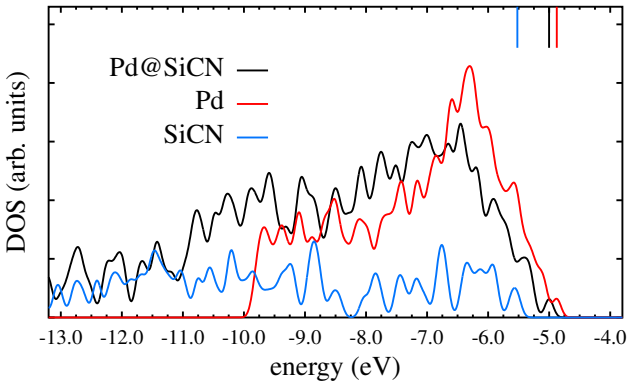

(a) $R = 5.5$ with PBE0

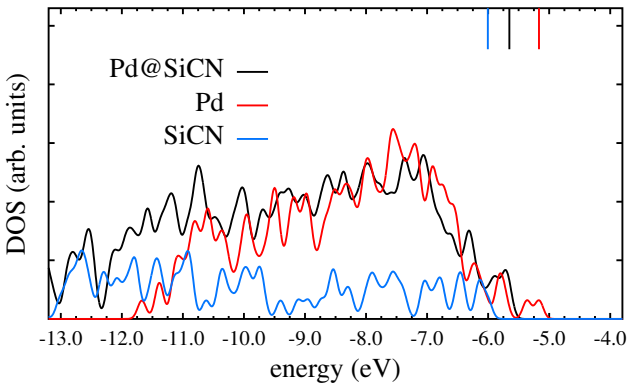

(b) $R = 5.5$ with BHLYP

Fig. 4 DFT DOS obtained with PBE0 (a) and BHLYP (b) for the subsystem with $R = 5.5$ for Pd only (red line), SiCN only (blue), and the combined Pd@SiCN (black).

Calculations using hybrid functionals are computationally more demanding because of the Fock integrals. However, because of the (fraction of) Fock exchange, hybrids are expected to eliminate important parts of the one-electron self-interaction error that may displace the energetic position of Kohn-Sham states in the DOS. It was repeatedly argued that functionals affected by electronic self-interaction erroneously shift states from localized orbitals to higher energies, while delocalized states suffer less from self-interaction[53,54,65–73]. In the context of Pd@SiCN, in particular the cancellation of self-interaction for localized orbitals originating from *d*-states is important[6,50,74,75].

The effect of counteracting self-interaction can clearly be seen in Fig. 4(a): in the DOS obtained with PBE0, which includes 25 % Fock exchange, a large number of states is shifted significantly towards lower energies in comparison to the PBE result shown in Fig. 3(b). This effect can also be seen in Fig. 2, since here the values for $\Sigma_\Delta(R)$ obtained with PBE0 are consistently smaller than the ones obtained with pure PBE. Using BHLYP with its 50 % of Fock exchange results in a even larger shift of states towards lower energies, as seen in Fig. 4(b).

However, despite the shifts in the DOS that the hybrid functionals introduce, the main conclusion from the PBE calculations is confirmed by the hybrid calculations: The energetically high-lying part of the DOS of Pd@SiCN originates mostly from the Pd atoms and the SiCN support has only a minor direct electronic effect on the DOS.

5 Conclusions

This study served a two-fold purpose. On the one hand, we tested a subsystem scheme for investigating the electronic structure of a particle partially embedded in a matrix. The scheme is useful when the total system is too large for a straightforward first principles calculation. Based on atomic positions that we obtained from classical MD, we calculated the electronic structure with DFT for subsystems of systematically increasing size with a common, diligently chosen reference point.

On the other hand, employing this scheme allowed us to obtain insight into the properties of a Pd nanoparticle that is partially embedded in a SiCN matrix. We found that the density of states in the chemically most relevant region, i.e., closely below the Fermi level, is dominated by states that originate from the Pd atoms. The SiCN support has only a small direct influence on the occupied density of states [*]. We verified that this finding does not depend on a specific choice of density functional, but is a general and thus reliable observation.

This finding is relevant for understanding why the Pd@SiCN system can serve as an efficient catalyst. In principle, there are two possibilities why embedding can influence catalytic efficiency. One option could be that the embedding changes the properties of the embedded particle, in particular at the surface, with either positive or detrimental consequences for the catalytic activity. The other option is that the support is irrelevant for the direct electronic properties, but contributes positively in catalytic applications because it provides mechanical support and stability, improves the nanoparticle handling and prevents coagulation. Our study shows that only the latter option is relevant in Pd@SiCN.

A Subsystem scaling

We here give further details about the subsystem construction, in particular on the scaling of the number of atoms and electrons with increasing subsystem size. In Fig. 5(a) the number of atoms is shown as a function of the radius R for the subsystems containing only Pd, only SiCN, and the combined Pd@SiCN. For these systems, the corresponding number of electrons, which is the relevant quantity to estimate the costs of a DFT calculation, is shown

[*] There may be some indirect influence when the embedded particle's geometry differs largely from the geometry of the free particle, but structural changes can be checked experimentally.

as a function of R in Fig. 5(b) (Note that for the SiCN support all electrons were taken into account, while for Pd only the 18 electrons of the valence shell were counted due to the pseudopotential representation in TURBOMOLE). Each curve is fitted by the function

$$f(R) = a \cdot R^b \tag{2}$$

and the values of the fitting parameter a and b are shown in the figure.

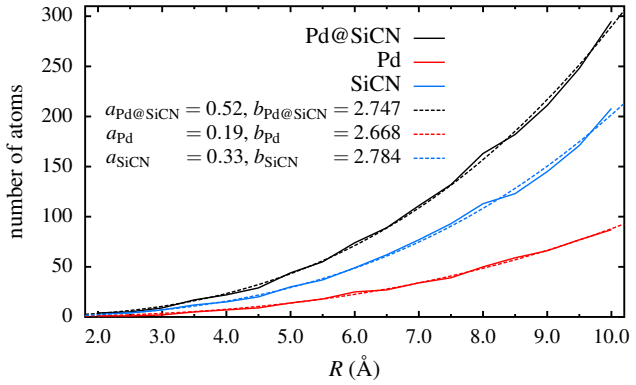

(a) Scaling of the number of atoms

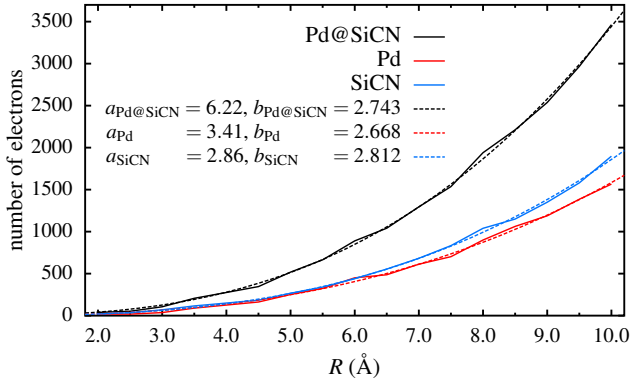

(b) Scaling of the number of electrons

Fig. 5 Scaling of the numbers of atoms (a) and electrons (b) with respect to the sphere radius R around the reference point for only Pd, only SiCN, and the combined system Pd@SiCN. Each curve is fitted according to Eq. (2) (dashed lines), and the corresponding values of the parameter a and b are shown in the graphs.

Fig. 5 shows that the values of b for the subsystems containing only Pd, only SiCN, and the combined Pd@SiCN, agree reasonably well. Therefore, at each radius R the ratio of Pd to SiCN atoms is more or less the same. This supports the idea of the subsystem construction.

Acknowledgments

Financial support from the Deutsche Forschungsgemeinschaft (DFG, via SFB 840, project B1), the German-Israel Foundation (GIF), and the Brazilian agencies FAPESP (grant 2014/02071-5) and CNPq (grant 305082/2013-2) is gratefully acknowledged.

References

1 J. Akola, M. Manninen, H. Häkkinen, U. Landman, X. Li and L.-S. Wang, *Phys. Rev. B*, 2000, **62**, 13216.

2 S. N. Khanna, M. Beltran and P. Jena, *Phys. Rev. B*, 2001, **64**, 235419.

3 R. Ferrando, J. Jellinek and R. L. Johnston, *Chem. Rev.*, 2008, **108**, 846–904.

4 M. Hakala, O. Pakarinen and A. Foster, *Phys. Rev. B*, 2008, **78**, 045418.

5 A. Logsdail, L. O. Paz-Borbón and R. L. Johnston, *J. Comp. Theo. Nano.*, 2009, **6**, 857.

6 C. J. Cramer and D. G. Truhlar, *Phys. Chem. Chem. Phys.*, 2009, **11**, 10757–10816.

7 S. Riikonen, A. S. Foster, A. V. Krasheninnikov and R. M. Nieminen, *Phys. Rev. B*, 2010, **81**, 125442.

8 I. C. Gerber, A. V. Krasheninnikov, A. S. Foster and R. M. Nieminen, *New J. Phys.*, 2010, **12**, 113021.

9 D. T. Tran and R. L. Johnston, *Proc. R. Soc. A*, 2011, **467**, 2004–2019.

10 L. Leppert and S. Kümmel, *J. Phys. Chem. C*, 2011, **115**, 6694–6702.

11 P. Ghosh, M. F. Camellone and S. Fabris, *J. Phys. Chem. Lett.*, 2013, **4**, 2256.

12 M. Aslan, J. B. A. Davis and R. L. Johnston, *Phys. Chem. Chem. Phys.*, 2016, **18**, 6676.

13 V. Kaydashev, P. Ferrari, C. Heard, E. Janssens, R. L. Johnston and P. Lievens, *Part. Part. Syst. Charact.*, 2016, **33**, 364–372.

14 J. Akola, M. Manninen, H. Häkkinen, U. Landman, X. Li and L.-S. Wang, *Phys. Rev. B*, 1999, **60**, R11297.

15 H. Häkkinen, M. Moseler, O. Kostko, N. Morgner, M. A. Hoffmann and B. V. Issendorff, *Phys. Rev. Lett.*, 2004, **93**, 093401.

16 J. K. Nørskov, T. Bligaard, J. Rossmeisl and C. H. Christensen, *Nat. Chem.*, 2009, **1**, 37–46.

17 R. B. Getman and W. F. Schneider, *ChemCatChem*, 2010, **2**, 1450–1460.

18 S. Ghosh, Q. Wang, G. P. Das and P. Jena, *Phys. Rev. B*, 2010, **81**, 235215.

19 L. Leppert, R. Q. Albuquerque, A. S. Foster and S. Kümmel, *J. Phys. Chem. C*, 2013, **117**, 17268–17273.

20 R. G. Capelo, L. Leppert and R. Q. Albuquerque, *J. Phys. Chem. C*, 2014, **118**, 21647–21654.

21 L. Leppert, R. Kempe and S. Kümmel, *Phys. Chem. Chem. Phys.*, 2015, **17**, 26140–26148.

22 H.-C. Weissker, O. Lopez-Acevedo, R. L. Whetten and X. López-Lozano, *J. Phys. Chem. C*, 2015, **119**, 11250–11259.

23 P. V. Cherepanov, I. Melnyk, E. V. Skorb, P. Fratzl, E. Zolotoyabko, N. Dubrovinskaia, L. Dubrovinsky, Y. S. Avadhut, J. Senker, L. Leppert, S. Kümmel and D. V. Andreeva, *Green Chem.*, 2015, **17**, 2745.

24 S. Matsuo, S. Yamazoe, J.-Q. Goh, J. Akola and T. Tsukuda, *Phys. Chem. Chem. Phys.*, 2016, **18**, 4822–4827.

25 X. Andrade, D. Strubbe, U. De Giovannini, A. H. Larsen, M. J. T. Oliveira, J. Alberdi-Rodriguez, A. Varas, I. Theophilou, N. Helbig, M. J. Verstraete, L. Stella, F. Nogueira, A. Aspuru-Guzik, A. Castro, M. A. L. Marques and A. Rubio, *Phys. Chem. Chem. Phys.*, 2015, **17**, 31371.

26 A. M. Doyle, S. K. Shaikhutdinov, S. D. Jackson and H. J. Freund, *Angew. Chem. Int. Ed.*, 2003, **42**, 5240–5243.

27 P. Pyykkö, *Angew. Chem. Int. Ed.*, 2004, **43**, 4412–4456.

28 A. S. K. Hashmi, *Chem. Rev.*, 2007, **107**, 3180–3211.

29 M. Schrinner, M. Ballauff, Y. Talmon, Y. Kauffmann, J. Thun, M. Möller and J. Breu, *Science*, 2009, **323**, 617–620.

30 J. Kaiser, L. Leppert, H. Welz, F. Polzer, S. Wunder, N. Wanderka, M. Albrecht, T. Lunkenbein, J. Breu, S. Kümmel, Y. Lu and M. Ballauff, *Phys. Chem. Chem. Phys.*, 2012, **14**, 6487–95.

31 R. Narayanan, *Molecules*, 2010, **15**, 2124–38.

32 D. Astruc, F. Lu and J. R. Aranzaes, *Angew. Chem. Int. Ed.*, 2005, **44**, 7852–7872.

33 J. M. Campelo, D. Luna, R. Luque, J. M. Marinas and A. A. Romero, *ChemSusChem*, 2009, **2**, 18–45.

34 R. J. White, R. Luque, V. L. Budarin, J. H. Clark and D. J. Macquarrie, *Chem. Soc. Rev.*, 2009, **38**, 481–94.

35 I. K. Sung, Christian, M. Mitchell, D. P. Kim and P. J. A. Kenis, *Adv. Funct. Mater.*, 2005, **15**, 1336–1342.

36 Y. Shi, Y. Wan and D. Zhao, *Chem. Soc. Rev.*, 2011, **40**, 3854–78.

37 G. Glatz, T. Schmalz, T. Kraus, F. Haarmann, G. Motz and R. Kempe, *Chem. Eur. J.*, 2010, **16**, 4231–4238.

38 M. Zaheer, T. Schmalz, G. Motz and R. Kempe, *Chem. Soc. Rev.*, 2012, **41**, 5102–16.

39 D. Forberg, J. Obenauf, M. Friedrich, S.-M. Hühne, W. Mader, G. Motz and R. Kempe, *Catal. Sci. Technol.*, 2014, **4**, 4188–4192.

40 R. Kempe and T. Schwob, *Angew. Chem. Int. Ed.*, 2016, accepted.

41 D. Forberg, T. Schwob, M. Zaheer, M. Friedrich, N. Miyajima and R. Kempe, *Nat. Commun.*, 2016, **7**, 132001.

42 M. Kamperman, A. Burns, R. Weissgraeber, N. Van Vegten, S. C. Warren, S. M. Gruner, A. Baiker and U. Wiesner, *Nano Lett.*, 2009, **9**, 2756–2762.

43 M. Zaheer, C. D. Keenan, J. Hermannsdörfer, E. Roessler, G. Motz, J. Senker and R. Kempe, *Chem. Mater.*, 2012, **24**, 3952–3963.

44 P. Hohenberg and W. Kohn, *Phys. Rev.*, 1964, **136**, B864–B871.

45 W. Kohn and L. J. Sham, *Phys. Rev.*, 1965, **140**, A1133–A1138.

46 R. G. Parr and W. Yang, *Density-Functional Theory of Atoms and Molecules*, Oxford University Press, New York, 1989.

47 J. P. Perdew, K. Burke and M. Ernzerhof, *Phys. Rev. Lett.*, 1996, **77**, 3865–3868.

48 J. P. Perdew, K. Burke and M. Ernzerhof, *Phys. Rev. Lett.*, 1997, **78**, 1396(E).

49 J. P. Perdew and A. Zunger, *Phys. Rev. B*, 1981, **23**, 5048–5079.

50 T. Schmidt and S. Kümmel, *Computation*, 2016, **4**, 33.

51 C. Adamo and V. Barone, *J. Chem. Phys.*, 1999, **110**, 6158–6170.

52 A. D. Becke, *J. Chem. Phys.*, 1993, **98**, 1372–1377.

53 T. Körzdörfer and S. Kümmel, *Phys. Rev. B*, 2010, **82**, 155206.

54 T. Schmidt and S. Kümmel, *Phys. Rev. B*, 2016, **93**, 165120–1–15.

55 R. Ferrando, G. Rossi, A. C. Levi, Z. Kuntova, F. Nita, A. Jelea, C. Mottet, G. Barcaro, A. Fortunelli and J. Goniakowski, *J. Chem. Phys.*, 2009, **130**, 174702–1 – 174702–9.

56 J. Goniakowski, A. Jelea, C. Mottet, G. Barcaro, A. Fortunelli, Z. Kuntová, F. Nita, A. C. Levi, G. Rossi and R. Ferrando, *J. Chem. Phys.*, 2009, **130**, 174703–1 – 174703–9.

57 M. S. Daw and M. Baskes, *Phys. Rev. B*, 1984, **29**, 6443–6453.

58 J. Tersoff, *Phys. Rev. B*, 1988, **37**, 6991–7000.

59 J. Tersoff, *Phys. Rev. B*, 1989, **39**, 5566(R).

60 J. Tersoff, *Phys. Rev. B*, 1990, **41**, 3248(E).

61 S. Plimpton, *J. Comput. Phys.*, 1995, **117**, 1–19.

62 `TURBOMOLE`, *V6.4 2012, a development of University of Karlsruhe and Forschungszentrum Karlsruhe 1989-2007, Turbomole GmbH since 2007; available from* `http://www.turbomole.com`.

63 A. Seidl, A. Görling, P. Vogl, J. A. Majewski and M. Levy, *Phys. Rev. B*, 1996, **53**, 3764–3774.

64 R. Ahlrichs, *Phys. Chem. Chem. Phys.*, 2004, **6**, 5119.

65 N. Dori, M. Menon, L. Kilian, M. Sokolowski, L. Kronik and E. Umbach, *Phys. Rev. B*, 2006, **73**, 195208.

66 S. Kümmel and L. Kronik, *Rev. Mod. Phys.*, 2008, **80**, 3–60.

67 N. Marom, O. Hod, G. E. Scuseria and L. Kronik, *J. Chem. Phys.*, 2008, **128**, 164107.

68 T. Körzdörfer, S. Kümmel, N. Marom and L. Kronik, *Phys. Rev. B*, 2009, **79**, 201205(R).

69 T. Körzdörfer, S. Kümmel, N. Marom and L. Kronik, *Phys. Rev. B*, 2010, **82**, 129903(E).

70 N. Marom and L. Kronik, *Appl. Phys. A*, 2009, **95**, 159–163.

71 T. Körzdörfer, *J. Chem. Phys.*, 2011, **134**, 094111–1–9.

72 D. A. Egger, S. Weissman, S. Refaely-Abramson, S. Sharifzadeh, M. Dauth, R. Baer, S. Kümmel, J. B. Neaton, E. Zojer and L. Kronik, *J. Chem. Theory Comput.*, 2014, **10**, 1934–1952.

73 L. Kronik and S. Kümmel, *First Principles Approaches to Spectroscopic Properties of Complex Materials*, Topics in Current Chemistry, Springer, Berlin, 2014.

74 Z. Szotek, W. M. Temmerman and H. Winter, *Phys. Rev. B*, 1993, **47**, 4029–4032.

75 T. C. Schulthess, W. M. Temmerman, Z. Szotek, W. H. Butler and G. M. Stocks, *Nat. Mater.*, 2005, **4**, 838–844.